www.ietdl.org

Published in IET Circuits, Devices & Systems
Received on 25th March 2014
Revised on 7th May 2014
Accepted on 15th May 2014
doi: 10.1049/iet-cds.2014.0069

Special Issue on Graphene Electronics

ISSN 1751-858X

Origin of 1/*f* noise in graphene produced for large-scale applications in electronics

Vidya Kochat[1], Anindita Sahoo[1], Atindra Nath Pal[1], Sneha Eashwer[1], Gopalakrishnan Ramalingam[2], Arjun Sampathkumar[2], Ryugu Tero[3], Tran Viet Thu[3], Sanjeev Kaushal[4], Hiroshi Okada[3,5], Adarsh Sandhu[3,5], Srinivasan Raghavan[2], Arindam Ghosh[1]

[1]*Department of Physics, Indian Institute of Science, Bangalore 560 012, India*
[2]*Materials Research Center, Indian Institute of Science, Bangalore 560 012, India*
[3]*Electronics Inspired Interdisciplinary Research Institute (EIIRIS), Toyohashi University of Technology, Toyohashi 441-8580, Japan*
[4]*Tokyo Electron Ltd, Minato-ku, Tokyo 107-6325, Japan*
[5]*Department of Electrical and Electronic Engineering, Toyohashi University of Technology, Toyohashi 441-8580, Japan*
E-mail: vidyakochat@physics.iisc.ernet.in

Abstract: The authors report a detailed investigation of the flicker noise (1/*f* noise) in graphene films obtained from chemical vapour deposition (CVD) and chemical reduction of graphene oxide. The authors find that in the case of polycrystalline graphene films grown by CVD, the grain boundaries and other structural defects are the dominant source of noise by acting as charged trap centres resulting in huge increase in noise as compared with that of exfoliated graphene. A study of the kinetics of defects in hydrazine-reduced graphene oxide (RGO) films as a function of the extent of reduction showed that for longer hydrazine treatment time strong localised crystal defects are introduced in RGO, whereas the RGO with shorter hydrazine treatment showed the presence of large number of mobile defects leading to higher noise amplitude.

1 Introduction

Graphene, which represents a truly two-dimensional (2D) material consisting of a single layer of C atoms, has attracted much attention owing to its unique electronic properties [1, 2]. Ballistic transport with extremely high mobilities of above 2×10^5 cm^2/Vs have been reported in suspended graphene [3] and on boron nitride substrate [4] facilitating studies on many exotic physical phenomena unique to graphene. Apart from the fundamental physics, graphene also has potential applications as transparent electrodes in solar cells [5], as ultra-highfrequency transistors [6], in flexible electronics and optoelectronics [7, 8] and as sensors [9, 10]. Even though graphene obtained from micromechanical exfoliation of natural graphite is usually superior in quality and has been the backbone of most of the basic research, technological applicability of graphene relies in its large-scale production. Recent advances in this direction include epitaxial growth of graphene on SiC [11], thermal decomposition of hydrocarbon gases/liquids on transition metals by chemical vapour deposition (CVD) [12–14] and finally chemical exfoliation and reduction of graphene oxide (GO) [15]. Among these the most promising technique has been that of CVD because of its simplicity, cost-effectiveness and tunability to produce large-sized grains [16–18] and has resulted in industrial scale production of graphene films as large as 30 inches, which can be transferred onto any arbitrary substrate [19]. Another method which has recently attracted immense interest is the chemical reduction of GO. Even though reduced graphene oxide (RGO) has much lower mobilities compared with the graphene grown from CVD and epitaxial methods, by reducing the extent of disorder, RGO can be used efficiently in nanoelectronics applications [20–22].

The main challenge in the implementation of CVD grown graphene is its polycrystallinity, which can affect the electrical, mechanical and thermal properties of the otherwise pristine graphene film and have been shown to lead to strong carrier scattering at the grain boundaries resulting in lower mobilities and localisation behaviour [23–31]. However, a recent series of experiments have established that the electrical and mechanical properties of the graphene grain boundaries are governed entirely by the arrangement of the defects at the boundary and can even result in an enhancement of the properties for good interdomain connectivity [32, 33]. There could also be other structural defects in the large area graphene films, which originate during the polymer-assisted transfer of graphene from the Cu (or other transition metals) foil to the substrate. These Stone–Wales defects and the grain boundaries are known to be very reactive and can adsorb

chemical species which can also result in enhanced scattering [34]. Although this could be made useful for applications like sensing, they could considerably degrade the electronic transport.

An important aspect of the grain boundaries, which remains essentially unknown but governs the device utility for sensing and other nanoelectronic applications is the intrinsic electrical noise known as the 'flicker' noise or the $1/f$ noise. The $1/f$ noise depends on the nature and dynamics of the disorder and provides information that is very different from that obtained from time-averaged transport. In the case of polycrystalline graphene, it is thus very important to understand and quantify the noise levels arising from the grain boundaries and other structural disorder. In RGO, it has been observed that the presence of chemical disorder like oxygen functional groups leads to the formation of localised states and can significantly degrade the electronic transport [21, 22]. The effect of the localised states on the electronic transport of various 2D layered materials have been studied previously [35, 36]. In this article, we study the origin of $1/f$ noise in large area graphene films grown by CVD technique and those obtained by chemical reduction of GO. We find that the $1/f$ noise in polycrystalline CVD grown graphene is significantly larger than in exfoliated graphene films. In the case of RGO, a detailed investigation of the nature as well as the kinetics of disorder was carried out using low-frequency noise measurements.

2 Sample fabrication and characterization

2.1 CVD grown graphene

The large-scale graphene films synthesised using the CVD technique are typically polycrystalline, and this arises because of the uncontrolled nucleation of graphene domains on the defect sites in Cu, which subsequently grow and coalesce to form a polycrystalline film. Cu is preferred over the other transition metals because of its low solubility of C which results in predominantly single layers of graphene. Recent studies have concentrated on studying the various growth space parameters such as the temperature, precursor gas flow rates and partial pressures which can result in larger sized grains of graphene [17, 18]. Later, it was reported that low-pressure CVD growth of graphene inside copper enclosures resulted in single-layer graphene grains of sizes reaching up to 0.5 mm [16]. This was followed by a surge of various techniques to obtain millimetre-sized single grains of graphene by improving the surface morphology of copper through electropolishing and annealing [37, 38]. In our experiments, we have varied the annealing time of the Cu foil prior to graphene growth which reduces the defect sites and thus results in lower nucleation of graphene domains and larger growth rate giving rise to large-sized grains. The CVD graphene was grown by the thermal decomposition of methane gas in the presence of H_2 gas (5 sccm CH_4: 1000 sccm of H_2) at 1000°C for 30 s on 99.8% pure Cu foil. The pre-annealing time of the Cu foils were varied from 5 min to 5 h leading to the results shown in Fig. 1*a*. For a pre-anneal time of 5 min, we find that there is a large density of graphene nucleations, which reduces considerably with increase in the pre-anneal time to 2 h where we also observe larger single crystal grains because of faster growth rate. Finally, for large pre-anneal time of 5 h, we see a complete graphene film coverage on Cu. These graphene films consist of 90% single-layer graphene and a few multilayer patches, which grow especially at the nucleation sites. The Raman characterisation (with green laser of $\lambda \sim 514.5$ nm) of the graphene films on Cu showed a large D peak (at 1350 cm^{-1}) at the grain boundary region, whereas inside a single grain the D peak was absent as can be seen from Fig. 1*b*. This is an indication that the grain boundaries can act as strong short-range scattering centres. Graphene grown on Cu foil was transferred onto Si/SiO_2 wafer by coating poly(methyl methacrylate) (PMMA) on the graphene/Cu foil which was followed by etching out the Cu in ferric chloride solution (1.75 g of $FeCl_3$/5 ml of concentrated HCl/50 ml deionised water). The PMMA/graphene film was then rinsed thoroughly in deionised water and then transferred onto Si/SiO_2 wafer after which the PMMA was dissolved using acetone leaving graphene on SiO_2. Metal contacts on the transferred graphene were defined using standard e-beam lithography followed by thermal deposition of 50 nm of Au or 10 nm Ti/50 nm Au. The standard resistance against gate voltage characteristics of one such device with Si as the backgate is shown in Fig. 1*c* for various temperatures in which the sheet carrier density (n) was estimated from the gate capacitance. We observe field-effect mobilities ranging from ~ 400 to 1500 cm^2/Vs in our devices of CVD grown single layer graphene (SLG) on SiO_2, which is much lower than that of exfoliated graphene on SiO_2 [1, 2] and is the consequence of the polycrystalline nature of the CVD grown graphene films.

2.2 Reduced graphene oxide

GO was chemically exfoliated from graphite powder by modified Hummer's method [39, 40] and dropcasted on SiO_2 (90 nm)/Si(n^{++}) substrate. After that the oxygen functional groups of GO were reduced with hydrazine vapour at 100°C for different durations of treatment time [41]. Here, we have used three types of samples: (i) GO, (ii) reduced GO with 5 min of hydrazine treatment (RGO:5) and (iii) reduced GO with 30 min of hydrazine treatment (RGO:30). Fig. 2*a* shows the Raman spectroscopy of these three types of samples with highly intense D peak indicating extensive structural disorder in the samples [42]. Interestingly, the intensity of D peak of RGO:30 is much more than that of RGO:5 and GO. We have plotted the value of the ratio of the intensity of D peak to that of G peak (I_D/I_G) for three samples as a function of the time of hydrazine treatment in Fig. 2*b*, which shows that on an average the value of I_D/I_G is more in the case of RGO:30 than the others. This indicates that hydrazine treatment for longer time introduces more disorder through localised crystal defects leading to the reduction of in-plane sp^2 domain size because of extensive reduction [43]. We find that the I_D/I_G ratios of RGO:30 and RGO:5 have a median value of 1.19 and 1.17, with a range of variation of $1.19^{+0.2}_{-0.1}$ and 1.17 ± 0.1 around this median value, respectively. However, the relative standard deviations of I_D/I_G about the average values for GO and RGO are about 4 and 8%, respectively, which indicates that the fabrication process of RGO and GO is quite reproducible.

To measure the transport properties, contact pads were made on GO and RGO through standard e-beam lithography followed by thermal evaporation of 10 nm Cr/50 nm Au. At room temperature, the source–drain current (I_{SD}) of the samples RGO:30 and RGO:5 measured by varying the back-gate voltage (V_{BG}) showed a large hysteresis as shown in Figs. 2*c* and *d*. The origin of such

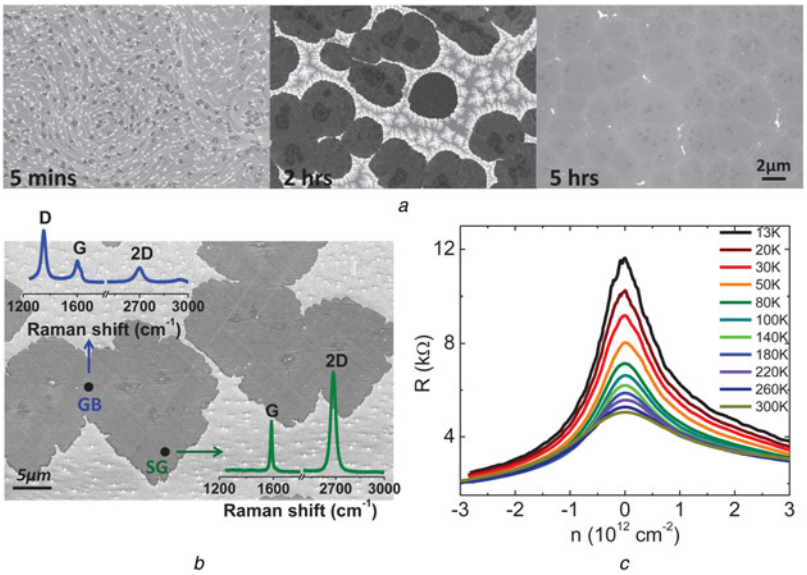

Fig. 1 *Sample fabrication and characterisation of CVD grown graphene*

a SEM images showing graphene growth on Cu foil where the pre-annealing time of Cu prior to graphene growth was changed to 5 min, 2 h and 5 h, respectively
b Comparison of Raman spectra obtained at the grain boundary region (GB) and inside a single grain (SG) shows a large D peak signifying large disorder at the grain boundary
c Standard R–V_g characteristics for polycrystalline CVD grown graphene is shown for different temperatures

large hysteresis can be attributed to the charge traps present at the interface of RGO (GO) and the SiO_2 substrate [44, 45] and the adsorbed water molecules by SiO_2 and RGO [46]. Since hydrazine treatment cannot reduce all the oxygen groups present in the GO sheets, these internal charged impurities can also contribute to the large hysteresis observed in I_{SD} with changing V_{BG}. Hydrazine treatment introduces some nitrogen doping in RGO through reaction with the carbonyl groups of GO resulting in electron doping which gives Dirac point at negative back-gate voltages [43, 47]. We also find that the resistance of the unreduced GO which is in the order of gigaohm, decreases to the order of megaohm in

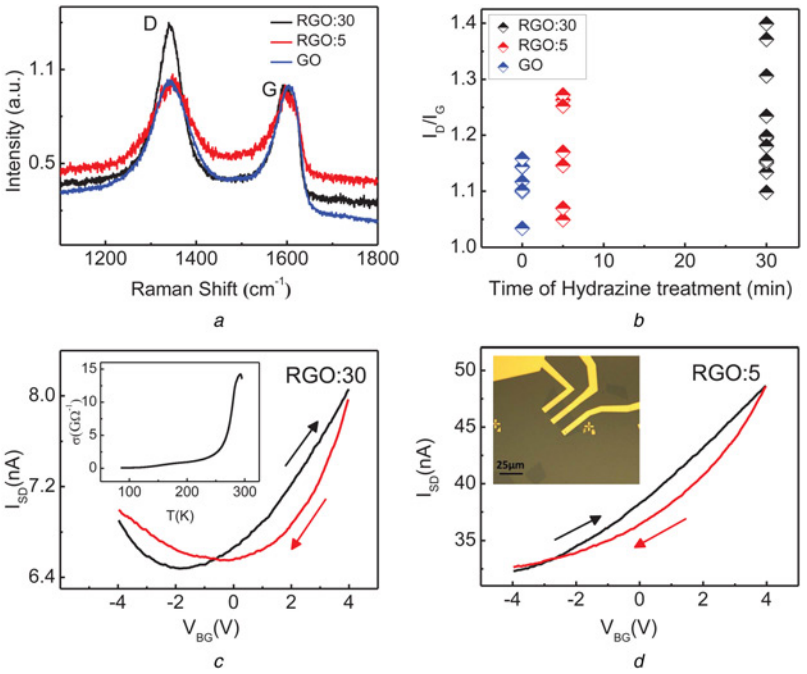

Fig. 2 *Sample fabrication and characterisation of GO and RGO*

a Raman spectroscopy of RGO:30, RGO:5 and GO which shows that the intensity of D peak of RGO:30 is more than that of others
b Ratio of intensity of D peak to the intensity of G peak (I_D/I_G) for all three samples with different timescales of hydrazine treatment
I_{SD} against V_{BG} plot of
c RGO:30 and
d RGO:5
The direction of arrows indicates the sweep direction of V_{BG}. The inset in (*c*) and (*d*) show the conductivity (σ) of the RGO:30 sample as a function of temperature and a typical device structure of RGO:5, respectively

doi: 10.1049/iet-cds.2014.0069

RGO:30 and RGO:5 as GO undergoes the hydrazine treatment. The conductivity of these samples increases with increasing temperature as depicted in the inset of Fig. 2*c*, indicating the insulating behaviour of these highly disordered samples.

3 Experiment

The 1/*f* noise in the CVD graphene devices were measured using an AC four-probe Wheatstone bridge configuration with a dual-channel Lock-in amplifier (SR830) [48] under high vacuum conditions as is shown in the schematic in Fig. 3*a*. The sample was biased by an AC carrier signal generated by the internal oscillator of the LIA. The output voltage from the sample is amplified by using a low-noise voltage preamplifier (SR560), which after balancing across a standard resistor is recorded by the lock-in amplifier (LIA) at two different phases. The in-phase component (recorded in X) is the sum of the sample signal and the background, whereas the quadrature component (recorded in Y) consists of only the background. The normalised resistance fluctuations obtained from voltage fluctuations at the LIA output as a function of time is shown in Fig. 3*b* for different carrier densities (n) in CVD graphene whose R–V_g characteristics is plotted in the inset of Fig. 3*c*. This time series data is then digitised and undergoes multistage decimation followed by digital processing using fast Fourier transform to finally obtain the power spectral density (PSD). The background noise obtained from the Y-component is then subtracted to obtain the noise power spectrum from the sample alone. In case of RGO, because of its very high resistance (of the order of megaohm) we derived current PSD by measuring low-frequency current fluctuations in a two-probe geometry while applying a constant amplitude AC source–drain voltage using lock-in amplifier. The normalised PSD for CVD graphene (S_R/R^2) and RGO (S_I/I^2) at different carrier densities are plotted in Fig. 3*c* and *d*, respectively. The inset in Fig. 3*d* displays the value of the noise exponent α for the RGO device which remains in between 1.1 and 1.25 at different V_{BG}. In both the cases, the noise spectra showed 1/*f* characteristics indicating the presence of mobile disorder with a wide distribution of time scales.

4 Results and discussions

The normalised PSD, S_R/R^2 at 1 Hz is plotted as a function of carrier density for exfoliated SLG and CVD grown SLG on SiO_2 in Figs. 4*a* and *b*, respectively. We clearly see that in both the cases the noise is maximum at lower n and decreases at higher n. Earlier reports attribute the origin of noise in graphene to the trapping–detrapping of carriers by the charged traps at the oxide interface and also because of the rearrangement of the trapped charges within the substrate leading to random fluctuations in the scattering cross-section [49–53]. At higher densities, because of the enhanced screening of these traps by the carriers in graphene, the sensitivity of graphene resistance to these processes is weakened leading to lower noise levels. Since these processes follow an activated behaviour, we expect the noise in these devices to increase at higher temperatures. This behaviour was indeed observed and is plotted in the inset of Fig. 4*b*.

To understand the effect of the various structural disorder on continuous polycrystalline films of graphene, we fabricated devices where the length of the graphene channel between the voltage probes were varied from <1 to 100 µm. A comparison of the noise levels for different channel

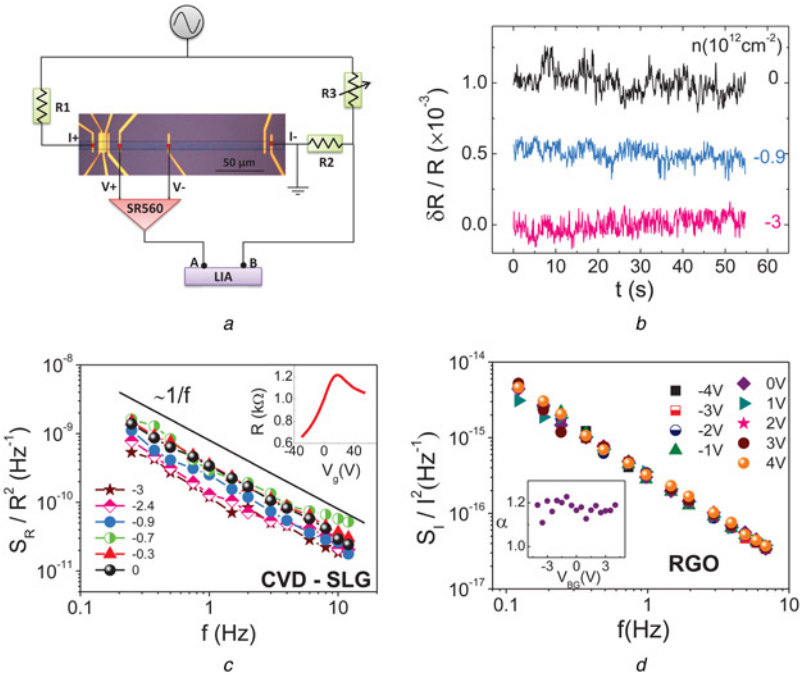

Fig. 3 *Noise measurement scheme*

a Optical image of a typical measured device showing the Wheatstone bridge arrangement for noise measurements
b Time series of resistance fluctuations in the CVD-SLG device at different densities, $n(10^{12}\ cm^{-2})$
c Normalised PSD at various densities is shown for the CVD-SLG device whose R–V_g is given in the inset
d Power spectra of 1/*f* noise normalised with the source–drain current at different back-gate voltages of RGO:30 at room temperature
The inset displays the value of the exponent α which remains in between 1.1 and 1.25 at different V_{BG} representing the 1/*f* noise

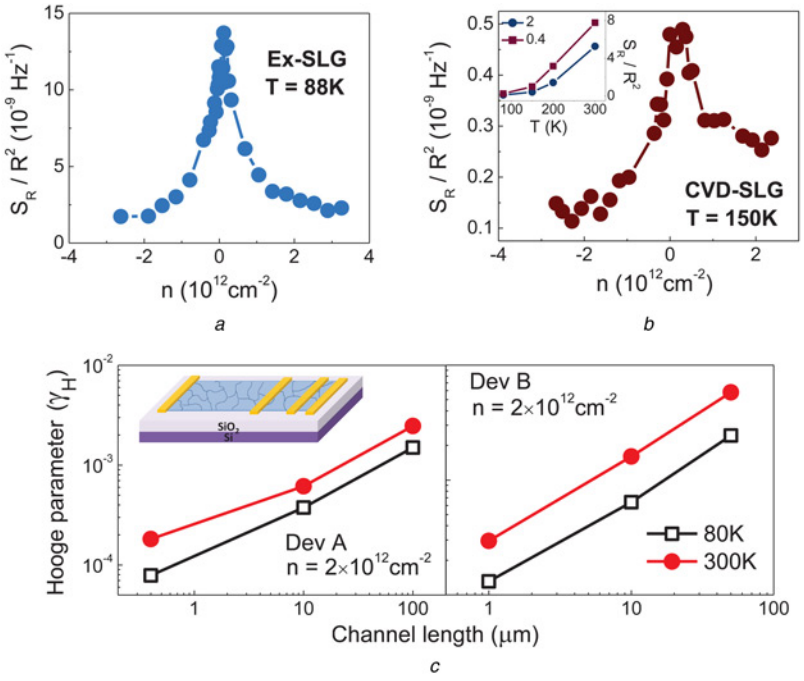

Fig. 4 *Noise in CVD grown graphene*

a Normalised PSD, S_R/R^2 at 1 Hz as a function of density is plotted for exfoliated SLG on SiO_2 at $T = 88$ K
b S_R/R^2 at 1 Hz as a function of density for CVD grown SLG on SiO_2 at $T = 150$ K
The inset shows noise as a function of temperature displaying activated behaviour
c Dependence of noise characterised by γ_H as a function of the length of the graphene channel between the voltage probes is shown for two devices, Dev A and Dev B at $n = 2 \times 10^{12}$ cm^{-2} for temperatures 80 and 300 K
The inset in (*c*) shows the schematic of the measured devices where the number of grain boundaries increases progressively for larger channel lengths leading to huge increase in γ_H

lengths is made by using the phenomenological Hooge parameter given by

$$\gamma_H = nAf^{\alpha} \times (S_R/R^2) \quad (1)$$

where A is the area of graphene between the voltage leads. The γ_H as a function of channel length calculated at $n = 2 \times 10^{12}$ cm^{-2} for two devices, Dev A and Dev B is shown in Fig. 4*c* at temperatures 80 and 300 K. We observe almost an order of magnitude reduction in the Hooge parameter for graphene channels of length ≤ 1 μm. The inset of Fig. 4*c* shows the schematic of the measured devices which illustrates that the number of grain boundaries and other structural defects are lower in the shorter channels, whereas in the longer channels they dominate the noise characteristics of the graphene channel.

CVD grown SLG is known to be intrinsically disordered because of the grain boundaries formed during growth and the point defects and inhomogeneities generated during the mechanical transfer process from Cu foil to SiO_2 wafer. It has been shown theoretically that the extended lattice defects like edges and grain boundaries can give rise to localised states near the Fermi energy, which can result in charge transfer between the grain boundary and the bulk via 'self-doping' [54, 55]. Also since the grain boundaries are chemically more reactive because of larger binding energies and the presence of dangling bonds, they could serve as preferential adsorption sites for many functional groups which could also lead to additional doping [34, 56]. We believe that the noise in CVD grown SLG is largely because of the above two reasons in addition to the charged traps in the SiO_2 substrate. The fluctuations in the number

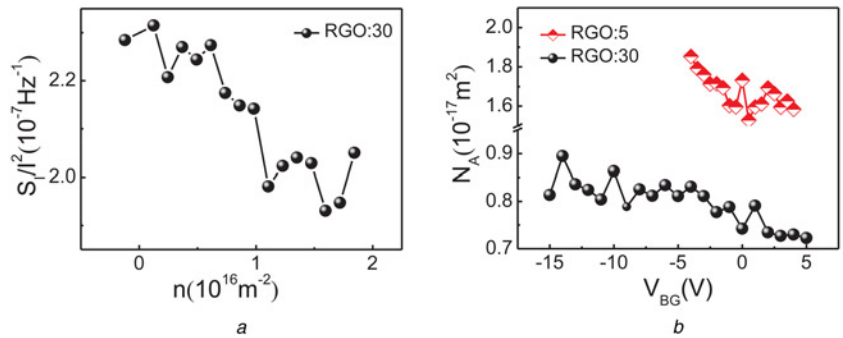

Fig. 5 *Noise in reduced graphene oxide films*

a Variance of noise power spectra normalised with the source–drain current (S_I/I^2) plotted as a function of carrier density (n) of RGO:30 at room temperature
b Noise amplitude, N_A[= (S_I/I^2) × area of the sample] at different back-gate voltages of both RGO:30 and RGO:5

doi: 10.1049/iet-cds.2014.0069

of carriers because of the trapping–detrapping processes at the grain boundary along with the fluctuations in the potential barrier at the grain boundary could result in large noise across the grain boundary in graphene [57]. Apart from the grain boundaries, the other sources of structural defects are the vacancies, ripples and multilayer patches which would depend on the growth space parameters and the transfer processes. This proves beyond doubt that more attention is needed in growing larger single crystal grains of graphene if we have to use CVD grown graphene for low-noise electronic device applications.

The structural defects have a common presence in the large area graphene films, regardless of the growth technique and transfer conditions. Next, we investigate the role of chemical defects in the transport of RGO films through $1/f$ noise. The low-frequency noise measurements were performed on two probe devices of both RGO:30 and RGO:5 in a high vacuum environment at room temperature. We have plotted the noise magnitude, which is the normalised PSD (S_I/I^2), as a function of carrier density (n) of the sample RGO:30 as depicted in Fig. 5*a*. Fig. 5 clearly indicates that the dominant noise mechanism in the RGO devices is very different from CVD or exfoliated graphene. As the carrier density increases, the reduction of noise magnitude can be observed, although the decrease is much weaker in this case. It is possible that because of extensive chemical disorder, the charge distribution in RGO is highly inhomogeneous and the change in gate voltage does not affect the overall screening much. Interestingly, we can see in Fig. 5*b* that the noise amplitude $N_A[=(S_I/I^2)\times$ area of the sample] of RGO:5 is almost two times larger than that of RGO:30 [58]. In RGO:5, all the oxygen functional groups might not have been removed because of the shorter time of hydrazine treatment (5 min). The remaining oxygen functional groups are weakly bonded to the RGO sheets and this chemical disorder could probably be attributed as the mobile defects in RGO:5 leading to a larger noise amplitude. In RGO:30, hydrazine treatment for longer time introduces greater density of localised structural defects as observed in Raman spectroscopy. Kinetics of these structural defects are likely to involve much larger energy barriers, resulting in relatively lower noise amplitude.

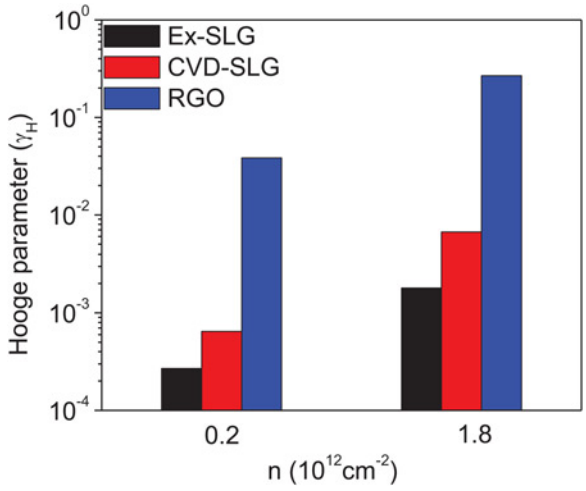

Fig. 6 *Comparison of the actual noise levels made by calculating the Hooge parameter, γ_H for the three cases, (i) Ex-SLG, (ii) CVD-SLG and (iii) RGO is plotted for densities 0.2 and 1.8×10^{12} cm^{-2} at 300 K*

Finally, we compare the noise levels of CVD grown SLG and RGO films with that of exfoliated graphene. In Fig. 6, the Hooge parameter at 300 K for the three devices are plotted at carrier densities, $n=0.2$ and 1.8×10^{12} cm^{-2}. We find that the noise in CVD grown graphene is much larger than the noise in exfoliated graphene because of the presence of grain boundaries and other structural defects which arises during the growth and the mechanical transfer processes. The noise in RGO is almost two orders of magnitude higher than disordered CVD grown graphene. This can be attributed to the presence of mobile defects in RGO in the form of chemical disorder such as oxygen functional groups and structural defects created by hydrazine reduction.

5 Conclusion

In conclusion, we have investigated the noise performance of large area graphene films grown by CVD and reduction of GO and identified the possible sources of disorder in these films. We observe that the kinetics and magnitude of disorder in RGO are strongly affected by the duration of hydrazine treatment. Hydrazine treatment for longer time creates localised lattice defects, whereas shorter time of hydrazine treatment introduces a large number of mobile defects as evident from Raman spectroscopy and noise measurements. To obtain high-mobility RGO, characterising the defect dynamics in RGO for various durations of hydrazine treatment is absolutely essential. In the case of polycrystalline graphene films grown by CVD, we infer that the grain boundaries and other structural defects act as the major source of noise because of the trapping–detrapping of charge carriers at these defect sites. Although this feature of the grain boundaries could be exploited for sensors, it needs to be addressed for other electronic applications that require lower noise levels.

6 Acknowledgments

We acknowledge the Department of Science and Technology (DST) and Tokyo Electron Limited for a funded project. V.K. and A.N.P. thank CSIR for financial support.

7 References

1 Novoselov, K.S., Geim, A.K., Morozov, S.V., *et al.*: 'Two-dimensional gas of massless Dirac fermions in graphene', *Nature*, 2005, **438**, pp. 197–200
2 Zhang, Y., Tan, Y-W., Stormer, H.L., Kim, P.: 'Experimental observation of the quantum Hall effect and Berry's phase in graphene', *Nature*, 2005, **438**, pp. 201–204
3 Bolotin, K.I., Sikes, K.J., Jiang, Z., *et al.*: 'Ultrahigh electron mobility in suspended graphene', *Solid State Commun.*, 2008, **146**, pp. 351–355
4 Dean, C.R., Young, A.F., Meric, I., *et al.*: 'Boron nitride substrates for high-quality graphene electronics', *Nat. Nanotechnol.*, 2010, **5**, pp. 722–726
5 Kim, K.S., Zhao, Y., Jang, H., *et al.*: 'Large-scale pattern growth of graphene films for stretchable transparent electrodes', *Nature*, 2009, **457**, pp. 706–710
6 Lin, Y.-M., Dimitrakopoulos, C., Jenkins, K.A. *et al.*.: '100-GHz transistors from wafer-scale epitaxial graphene', *Science*, 2010, **327**, p. 662
7 Roy, K., Padmanabhan, M., Goswami, S., *et al.*: 'Graphene-MoS2 hybrid structures for multifunctional photoresponsive memory devices', *Nat. Nanotechnol.*, 2013, **8**, pp. 826–830
8 Roy, K., Padmanabhan, M., Goswami, S., Phanindra Sai, T., Kaushal, S., Ghosh, A.: 'Optically active heterostructures of graphene and ultrathin MoS2', *Solid State Commun*, 2013, **175176**, pp. 735–42
9 Schedin, F., Geim, A.K., Morozov, S.V., *et al.*: 'Detection of individual gas molecules adsorbed on graphene', *Nat. Mater.*, 2007, **6**, pp. 652–655

10 He, Q., Wu, S., Yin, Z., Zhang, H.: 'Graphene-based electronic sensors', *Chem. Sci.*, 2012, **3**, pp. 1764–1772
11 de Heer, W.A., Berger, C., Ruan, M., *et al.*: 'Large area and structured epitaxial graphene produced by confinement controlled sublimation of silicon carbide', *Proc. Natl Acad. Sci.*, 2011, **108**, pp. 16900–16905
12 Li, X., Cai, W., An, J., *et al.*: 'Large-area synthesis of high-quality and uniform graphene films on copper foils', *Science*, 2009, **324**, pp. 1312–1314
13 Reina, A., Jia, X., Ho, J., *et al.*: 'Large area, few-layer graphene films on arbitrary substrates by chemical vapor deposition', *Nano Lett.*, 2009, **9**, pp. 30–35
14 Li, Z., Wu, P., Wang, C., *et al.*: 'Low-temperature growth of graphene by chemical vapor deposition using solid and liquid carbon sources', *ACS Nano*, 2011, **5**, pp. 3385–3390
15 Eigler, S., Enzelberger-Heim, M., Grimm, S., *et al.*: 'Wet chemical synthesis of graphene', *Adv. Mater.*, 2013, **25**, pp. 3583–3587
16 Li, X., Magnuson, C.W., Venugopal, A., *et al.*: 'Large-area graphene single crystals grown by low-pressure chemical vapor deposition of methane on copper', *J. Am. Chem. Soc.*, 2011, **133**, pp. 2816–2819
17 Li, X., Magnuson, C.W., Venugopal, A., *et al.*: 'Graphene films with large domain size by a two-step chemical vapor deposition process', *Nano Lett.*, 2010, **10**, pp. 4328–4334
18 Zhou, H., Yu, W.J., Liu, L., *et al.*: 'Chemical vapour deposition growth of large single crystals of monolayer and bilayer graphene', *Nat. Commun.*, 2013, **4**, pp. 3096
19 Bae, S., Kim, H., Lee, Y., *et al.*: 'Roll-to-roll production of 30-inch graphene films for transparent electrodes', *Nat. Nanotechnol.*, 2010, **5**, pp. 574–578
20 Chua, C.K., Pumera, M.: 'Chemical reduction of graphene oxide: a synthetic chemistry viewpoint', *Chem. Soc. Rev.*, 2014, **43**, pp. 291–312
21 Gmez-Navarro, C., Weitz, R.T., Bittner, A.M., *et al.*: 'Electronic transport properties of individual chemically reduced graphene oxide sheets', *Nano Lett.*, 2007, **7**, pp. 3499–3503
22 Eda, G., Fanchini, G., Chhowalla, M.: 'Large-area ultrathin films of reduced graphene oxide as a transparent and flexible electronic material', *Nat. Nanotechnol.*, 2008, **3**, pp. 270–274
23 Zhang, H., Lee, G., Gong, C., Colombo, L., Cho, K.: 'Grain boundary effect on electrical transport properties of graphene', *J. Phys. Chem. C*, 2010, **118**, pp. 2338–2343
24 Yu, Q., Jauregui, L.A., Wu, W., *et al.*: 'Control and characterization of individual grains and grain boundaries in graphene grown by chemical vapour deposition', *Nat. Mater.*, 2011, **10**, pp. 443–449
25 Fei, Z., Rodin, A.S., Gannett, W., *et al.*: 'Electronic and plasmonic phenomena at graphene grain boundaries', *Nat. Nanotechnol.*, 2013, **8**, pp. 821–825
26 Koepke, J.C., Wood, J.D., Estrada, D., *et al.*: 'Atomic-scale evidence for potential barriers and strong carrier scattering at graphene grain boundaries: a scanning tunneling microscopy study', *ACS Nano*, 2013, **7**, pp. 75–86
27 Cao, H., Yu, Q., Jauregui, L.A., *et al.*: 'Electronic transport in chemical vapor deposited graphene synthesized on Cu: quantum Hall effect and weak localization', *Appl. Phys. Lett.*, 2010, **96**, p. 122106
28 Ahmad, M., An, H., Kim, Y.S., *et al.*: 'Nanoscale investigation of charge transport at the grain boundaries and wrinkles in graphene film', *Nanotechnology*, 2012, **23**, p. 285705
29 Mesaros, A., Papanikolaou, S., Flipse, C.F.J., Sadri, D., Zaanen, J.: 'Electronic states of graphene grain boundaries', *Phys. Rev. B*, 2010, **82**, p. 205119
30 Yazyev, O.V., Louie, S.G.: 'Electronic transport in polycrystalline graphene', *Nat. Mater.*, 2010, **9**, pp. 806–809
31 Pal, A.N., Bol, A.A., Ghosh, A.: 'Large low-frequency resistance noise in chemical vapor deposited graphene', *Appl. Phys. Lett.*, 2010, **97**, p. 133504
32 Tsen, A.W., Brown, L., Levendorf, M.P., *et al.*: 'Tailoring electrical transport across grain boundaries in polycrystalline graphene', *Science*, 2012, **336**, pp. 1143–1146
33 Grantab, R., Shenoy, V.B., Ruoff, R.S.: 'Anomalous strength characteristics of tilt grain boundaries in graphene', *Science*, 2010, **330**, pp. 946–948
34 Malola, S., Häkkinen, H., Koskinen, P.: 'Structural, chemical, and dynamical trends in graphene grain boundaries', *Phys. Rev. B*, 2010, **81**, p. 165447
35 Ghatak, S., Pal, A.N., Ghosh, A.: 'Nature of electronic states in atomically thin MoS2 field-effect transistors', *ACS Nano*, 2011, **5**, pp. 7707–7712
36 Ghatak, S., Ghosh, A.: 'Observation of trap-assisted space charge limited conductivity in short channel MoS2 transistor', *Appl. Phys. Lett.*, 2013, **103**, p. 122103
37 Wang, H., Wang, G., Bao, P., *et al.*: 'Controllable synthesis of submillimeter single-crystal monolayer graphene domains on copper foils by suppressing nucleation', *J. Am. Chem. Soc.*, 2012, **134**, pp. 3627–3630
38 Yan, Z., Lin, J., Peng, Z., *et al.*: 'Toward the synthesis of wafer-scale single-crystal graphene on copper foils', *ACS Nano*, 2012, **6**, pp. 9110–9117
39 Ishikawa, R., Bando, M., Morimoto, Y., Park, S.Y., Sandhu, A.: 'Patterning of two-dimensional graphene oxide on silicon substrates', *Jpn. J. Appl. Phys.*, 2010, **49**, p. 06GC02
40 Tung, V.C., Allen, M.J., Yang, Y., Kaner, R.B.: 'High-throughput solution processing of large-scale graphene', *Nat. Nanotechnol.*, 2009, **4**, pp. 25–29
41 Tsuzuki, K., Okamoto, Y., Iwasa, S., Ishikawa, R., Sandhu, A., Tero, R.: 'Reduced graphene oxide as the support for lipid bilayer membrane', *J. Phys. Conf. Ser.*, 2012, **352**, p. 012016
42 Tuinstra, F., Koenig, J.L.: 'Raman spectrum of graphite', *J. Chem. Phys.*, 1970, **53**, pp. 1126–1130
43 Stankovich, S., Dikin, D.A., Piner, R.D., *et al.*: 'Synthesis of graphene-based nanosheets via chemical reduction of exfoliated graphite oxide', *Carbon*, 2007, **5**, pp. 1558–1565
44 Lee, Y.G., Kang, C.G., Jung, U.J., *et al.*: 'Fast transient charging at the graphene/SiO_2 interface causing hysteretic device characteristics', *Appl. Phys. Lett.*, 2011, **98**, p. 183508
45 Wang, H., Wu, Y., Cong, C., Shang, J., Yu, T.: 'Hysteresis of electronic transport in graphene transistors', *ACS Nano*, 2010, **4**, pp. 7221–7228
46 Kim, W., Javey, A., Vermesh, O., Wang, Q., Li, Y., Dai, H.: 'Hysteresis caused by water molecules in carbon nanotube field-effect transistors', *Nano Lett.*, 2003, **3**, pp. 193–198
47 Lv, R., Li, Q., Botello-Méndez, A.R., *et al.*: 'Nitrogen-doped graphene: beyond single substitution and enhanced molecular sensing', *Sci. Rep.*, 2012, **2**, p. 586
48 Ghosh, A., Kar, S., Bid, A., Raychaudhuri, A.K.: 'A set-up for measurement of low frequency conductance fluctuation noise using digital signal processing techniques'. eprint arXiv:cond-mat/0402130, 2004
49 Pal, A.N., Ghatak, S., Kochat, V., *et al.*: 'Microscopic mechanism of 1/f noise in graphene: role of energy band dispersion', *ACS Nano*, 2011, **5**, pp. 2075–2081
50 Pal, A.N., Ghosh, A.: 'Ultralow noise field-effect transistor from multilayer graphene', *Appl. Phys. Lett.*, 2009, **95**, p. 082105
51 Kochat, V., Goswami, S., Pal, A.N., Ghosh, A.: 'Physics of electrical noise in graphene', in Rao, C., Sood, A. (Eds.): 'Graphene: synthesis, properties, and phenomena' (Wiley-VCH Verlag GmbH Co. KGaA Press, 2012), pp. 159–195
52 Pal, A.N., Ghosh, A.: 'Resistance noise in electrically biased bilayer graphene', *Phys. Rev. Lett.*, 2009, **102**, p. 126805
53 Pellegrini, B.: '1/f noise in graphene', *Eur. Phys. J. B*, 2013, **86**, pp. 373
54 Peres, N.M.R., Guinea, F., Castro Neto, A.H.: 'Electronic properties of disordered two-dimensional carbon', *Phys. Rev. B*, 2006, **73**, pp. 125411
55 Lahiri, J., Lin, Y., Bozkurt, P., Oleynik, I.I., Batzill, M.: 'An extended defect in graphene as a metallic wire', *Nat. Nanotechnol.*, 2010, **5**, pp. 326–329
56 Tapaszt, L., Nemes-Incze, P., Dobrik, G., Jae Yoo, K., Hwang, C., Bir, L.P.: 'Mapping the electronic properties of individual graphene grain boundaries', *Appl. Phys. Lett.*, 2012, **100**, p. 053114
57 Dimitriadis, C.A., Farmakis, F.V., Kamarinos, G., Brini, J.: 'Origin of low-frequency noise in polycrystalline silicon thin-film transistors', *J. App. Phys.*, 2002, **91**, pp. 9919–9923
58 Robinson, J.T., Perkins, F.K., Snow, E.S., Wei, Z., Sheehan, P.E.: 'Reduced graphene oxide molecular sensors', *Nano Lett.*, 2008, **8**, pp. 3137–3140

doi: 10.1049/iet-cds.2014.0069